Stress-induced amorphization as a transformation plasticity mechanism demonstrated in forsterite

Jean Furstoss, Daniel Pino-Muñoz, Philippe Carrez, Pierre Hirel, Valentin Delbecq, Vahid Samaee, Hosni Idrissi, Patrick Cordier

communications materials

A Nature Portfolio journal

Article

https://doi.org/10.1038/s43246-025-01038-0

Stress-induced amorphization as a transformation plasticity mechanism demonstrated in forsterite

Jean Furstoss[1,6] ✉, Daniel Pino-Muñoz[2], Philippe Carrez[1], Pierre Hirel[1], Valentin Delbecq[1], Vahid Samaee[3,7], Hosni Idrissi[4] & Patrick Cordier[1,5]

Although stress-induced amorphization has recently been identified as a new and distinctive plasticity mechanism, a formal framework for its systematic application in materials engineering is still lacking. In this study, we establish that stress-induced amorphization in Mg_2SiO_4 forsterite exhibits all the key features of phase transformation plasticity, a well-known phenomenon that has enabled the development of high-performance materials. By analogy with the Transformation-Induced Plasticity (TRIP) effect, we introduce the concept of amorphous-TRIP (a-TRIP). We demonstrate that the a-TRIP features, in particular the orientation effect of stress-induced amorphization (particularly strong in forsterite), can be exploited to design materials with enhanced toughness, a notable advance for a class of materials traditionally limited by brittle behavior.

Recent experimental and computational studies have identified stress-induced amorphization as a potential driver of plasticity in materials where classical mechanisms, such as dislocation motion, are restricted or inhibited[1–4]. This phenomenon encompasses a diverse range of materials, including industrial ceramics such as boron carbide[5] and silicon carbide[6], intermetallic compounds[3,7], high-entropy alloys[8], and minerals such as quartz[9] and olivine[1]. Stress-induced amorphization is the result of the occurrence of mechanical instability, resulting in the formation and subsequent thickening of inter or intracrystalline amorphous shear bands[10]. Although this mechanism can lead to material failure[11], it can also enable ductile deformation[3] and may even induce significant changes in the material's rheological behavior near the glass transition temperature[1]. While previous studies have shown that stress-induced amorphization can act as a plasticity mechanism, a unified conceptual framework is still needed to fully characterize this phenomenon and exploit its potential applications in materials engineering.

Amorphization represents a phase transformation often accompanied by substantial density changes[12–14], a characteristic that aligns with the principles of transformation-induced plasticity (TRIP)[15–17]. TRIP is a well-established plasticity mechanism observed in a wide range of materials, from metallic systems[15,18] to minerals[19] and even ice[20]. This mechanism has paved the way for the development of advanced material classes, such as high-strength steels[21] and shape memory alloys[22]. The TRIP effect is primarily characterized by '[..] plastic flow arising from variations of the phase proportions'[23] or, equivalently, '[..] significantly increased plasticity during a phase change [..]'[24]. It generally manifests as a '[..] weakening of the mechanical properties of polycrystal, while it is undergoing a phase transformation [..]'[17]. Formally, the total shear strain-rate $\dot{\gamma}$ of a system consisting of a phase A transforming into phase B with phase proportion X, under shear can be partitioned following[17]:

$$\dot{\gamma} = \dot{\gamma}_A X + \dot{\gamma}_B (X - 1) + \alpha \dot{\gamma}_T, \tag{1}$$

where, $\dot{\gamma}_A$ and $\dot{\gamma}_B$ are the shear strain rate due to the flow of phases A and B themselves, α is an orientation averaging coefficient and $\dot{\gamma}_T$ is the shear strain-rate due to the phase transformation. Notably, all phase transformations described in TRIP studies to date have involved the transformation of a crystalline phase into an other crystalline phase. Here, we focus on the transformation of a crystalline phase into an amorphous material through the stress-induced amorphization mechanism.

Recent studies on stress-induced amorphization have generally assumed that the plastic flow associated with this mechanism stems from the deformation of the resulting weaker amorphous phase itself[2,3]. Here, we conduct an in-depth analysis of this mechanism within Mg_2SiO_4 system, a material with experimentally demonstrated susceptibility to both intracrystalline and grain boundary (GB) stress-induced amorphization[10,25]. By

[1]Univ. Lille, CNRS, INRA, ENSCL, UMR 8207, UMET, Unité Matériaux et Transformations, Lille, France. [2]Mines Paris, PSL Research University, CEMEF-Centre de mise en forme des matériaux, Sophia Antipolis, France. [3]Department of Physics, Electron Microscopy for Materials Science, University of Antwerp, Antwerp, Belgium. [4]Institute of Mechanics, Materials and Civil Engineering, UCLouvain, Louvain-la-Neuve, Belgium. [5]Institut Universitaire de France, Paris, France. [6]Present address: Université de Poitiers, ISAE-ENSMA, CNRS, PPRIME, Poitiers, France. [7]Present address: OCAS NV, Zelzate, Belgium.
✉e-mail: jean.furstoss@univ-poitiers.fr

studying strain partitioning during amorphization, crystallographic orientation effects, and changes in mechanical properties, we show that stress-induced amorphization exhibits the defining characteristics of a phase transformation plasticity and introduce the concept of amorphous-TRIP (a-TRIP). In addition to enhancing comprehension of stress-induced amorphization, these findings unveil novel avenues for mechanically driven GB engineering in polycrystalline materials.

We begin by analyzing strain partitioning in a molecular dynamics (MD) simulation of Mg_2SiO_4 polycrystal undergoing shear deformation, where three distinct plasticity mechanisms are observed (i.e. dislocation glide, amorphous flow and a-TRIP). We then demonstrate through a direct comparison between MD and finite element (FE) simulations that the amorphization phase transformation generates plastic strain by itself. Next, we investigate how crystallographic orientation affects the plastic strain generated by amorphization by studying, through a series of MD simulations, the behavior of an intracrystalline amorphous shear bands under stress. Finally, we examine GB stress-induced amorphization within a polycrystalline context using MD simulations, supported by high-resolution transmission electron microscopy (HRTEM) images of amorphized GBs in Mg_2SiO_4. This combined approach highlights the potential for mechanically driven GB engineering, thank to the orientation effect of a-TRIP.

Results and Discussion

Stress induced amorphization is a major contributor to plastic deformation

This study focuses on Mg_2SiO_4 forsterite, an iono-covalent orthorhombic mineral (space group *Pbnm*), which represents the magnesium-rich end member of the olivine solid solution $(Mg,Fe)_2SiO_4$, a primary constituent of the Earth's upper mantle. Like many low-symmetry ceramics, forsterite possesses a limited number of slip systems for dislocation glide[26–28], which are also subject to high lattice friction[29]. The restriction of dislocation glide as the sole mechanism for accommodating deformation has led to investigations into alternative plasticity mechanisms, such as dislocation-assisted GB sliding[30] or disclination-assisted dislocation creep[31]. More recently, several studies have revealed the formation of both amorphized GB[1] and intracrystalline amorphous shear bands[10,25] during the deformation of olivine. Indeed, HRTEM characterizations of deformed polycristalline olivine samples have confirmed that stress-induced amorphization is prevalent in this material deformed under high stress at low temperature. Furthermore, a close inspection of amorphized GBs reveals the occurrence of faceted amorphized GBs, as illustrated in Fig. 1a, featuring a (120) GB plane faceted with (100) and (010) planes.

Subsequently, we performed MD simulations of polycrystalline forsterite deformed by simple shear at constant strain rate of 10^8 s^{-1} at 300 K. The recently developed Steinhardt Gaussian Mixture Analysis (SGMA)[32] enables the identification of various types of local atomic environment in low-symmetry crystals, including dislocations, amorphous regions, and interfaces (hereafter referring to crystal/crystal interfaces, i.e., grain boundaries or amorphous/crystal interface). The results of the structural analysis for the initial system and after 25% shear deformation are presented in Fig. 1b. Extended details of the simulation and analysis performed in the following are given in the Methods section M.2.1. While the GBs are initially pristine, shear deformation triggers the amorphization of numerous GBs, even in the presence of dislocation nucleation and glide. This finding underscores the interplay between different plasticity mechanisms, highlighting the significant contribution of GB amorphization to the overall deformation of the polycrystal. More quantitatively, the analysis of the shear-strain partitioning across different regions of the polycrystal, as depicted in Fig. 1c, reveals that the amorphous/crystal interface regions contribute for most of the plastic strain (≈38%), followed by the crystalline regions (≈34%) and the amorphous regions (≈28%). This production of plastic strain at the amorphous/crystal interface is not limited to the initiation of plasticity but continues to increase throughout the macroscopic deformation.

This unexpected observation provides a new perspective on stress-induced amorphization as a deformation mechanism, by emphasizing the importance of the amorphous/crystal interface region in producing plastic strain during amorphization. This occurrence of significant plastic flow at the amorphous/crystal interface, as observed in our simulation, could be explained in two ways, either through the rheological contrast between the crystalline and the amorphous materials, or through the production of plastic deformation by the phase transformation such as for TRIP effect[17].

To elucidate this point, we analyzed the behavior of an intracrystalline amorphous layer subjected to shear, simulated with both FE and MD model. As an example, we present a system consisting in a (100) oriented amorphous band sheared in the [001] direction deformed at a constant shear strain rates of 10^{10} s^{-1} at 300 K (Fig. 2). The FE model incorporates both elastic behavior to represent the crystal regions (where no plasticity

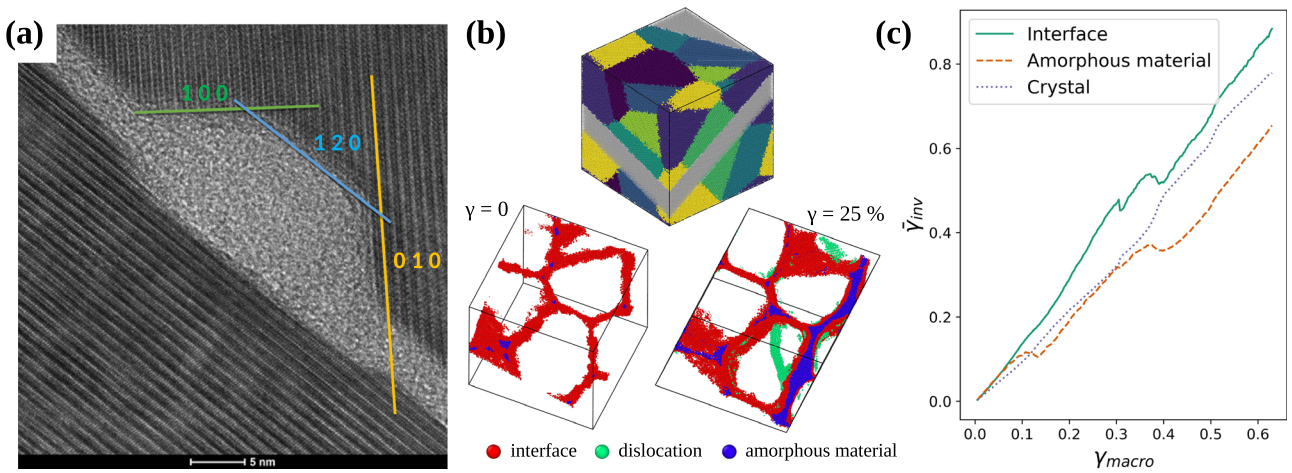

Fig. 1 | Importance of stress-induced amorphization in Mg_2SiO_4. a HRTEM micrograph of an amorphized GB in an olivine sample deformed at 300 MPa and 1473 K (see Method section M.1 for more details). **b** Visualization of a Mg_2SiO_4 polycrystal deformed, using molecular dynamics, in simple shear at constant strain rate of 10^8 s^{-1} and ambient temperature. Cross sections (corresponding to the light gray slice shown in the top figure) of the sample are compared for 0 % (left) and 25 % (right) of macroscopic shear strain. Ions are colored accordingly to their local atomic environments, atomic environment reflecting interface are displayed in red, dislocation lines in green, highly disorder environment reflecting amorphous rich region in blue. For clarity, crystalline environment is omitted. At a strain of $\gamma = 0.25$, intracrystalline plasticity mechanism is revealed through the appearance of dislocation lines and we also note a clear tendency of some GB (initially pristine as shown with the occurence of thin interface regions at $\gamma = 0$) to become thicker and amorphous. **c** volume averaged atomic shear strain invariant as defined in ref. 49 for the different regions of the polycrystal presented in (**b**) as a function of macroscopic shear strain.

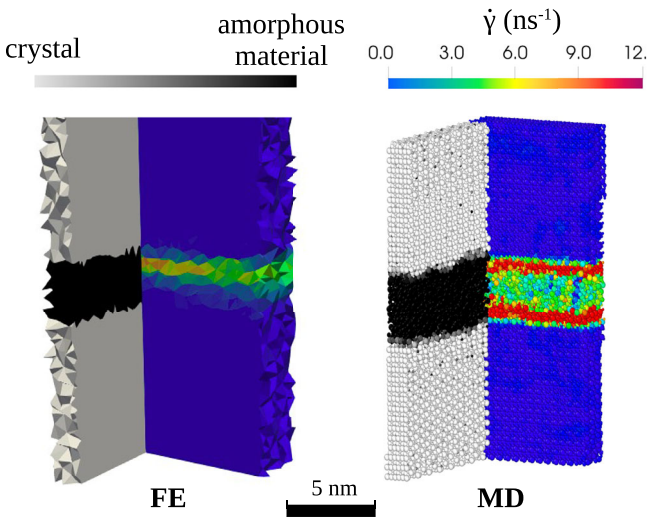

Fig. 2 | One-to-one comparison between Finite Element (FE) and Molecular Dynamics (MD) simulations of the shearing of an intragranular amorphous band at constant shear strain rate of 10^{10} s^{-1} at 300 K. The sheared plane is (100) and the shear direction is along the [001] axis. The gray colored scale represents the nature of the material (i.e., crystal in light gray and amorphous material in black) and the color scale bar represents the local plastic shear strain rate $\dot{\gamma}$.

mechanisms is observed in the MD simulations) and elasto-viscous flow to account for the amorphous behavior. The elastic constants were determined directly from MD simulations, while the viscous flow law was calibrated for Mg_2SiO_4 based on MD simulations with the same interatomic potential as described in ref. 33. The width and position of the amorphous region was fed into the FE simulation using data obtained from MD. In both models, the same constant shear strain rate was imposed by changing the shape of the simulation cell. It is important to note that no plasticity mechanism was assigned to the amorphous/crystal interface in the FE model. Additional details on the methodology can be found in the Methods section M.2.2.

A qualitative comparison of shear strain rates between the FE and MD simulations is presented in Fig. 2. Although the shear strain rates within the amorphous and crystalline regions are similar in both simulations, the high shear strain rates observed at the amorphous/crystal interfaces in the MD simulation are absent in the FE model. Moreover, the significant weakening observed in the MD simulations is completely absent from the FE model (see strain stress curve in Supplementary Fig. S.1), leading to an overestimation of the macroscopic shear stress by the FE model.

These results emphasize that amorphization itself produces plastic deformation and leads to a weakening of the mechanical properties of the material during phase transformation, which are two key aspects of the TRIP effect[17]. Moreover, in the polycrystalline shear simulation presented in Fig. 1b, c, the three shear strain-rate contributions of Eq. (1) (i.e., $\dot{\gamma}_A$ dislocation glide, $\dot{\gamma}_B$ amorphous flow, and $\dot{\gamma}_T$ a-TRIP) are of the same order of magnitude, emphasizing the need for the characterization of the shear strain-rate related to the crystal to amorphous phase transformation.

Small scale investigation of stress-induced amorphization

To further investigate this plasticity mechanism in Mg_2SiO_4, we turn to a systematic study of the a-TRIP effect in forsterite. Following the previous setup (Fig. 2), a series of MD simulations are performed to investigate the shear behavior of different intragranular amorphous bands, as illustrated in Fig. 3a. In this context, the crystallographic properties of the systems are denoted as (hkl)[hkl], where (hkl) refers to the crystal plane parallel to the amorphous band, and [hkl] indicates the shear direction within the crystallographic frame. We examined all combinations of $\{h00\} < 0k0 >$ as well as different initial amorphous thicknesses. Constant shear stress simulations were performed over a range of shear stresses (between 2 and 2.6 GPa) and temperatures (between 300 and 900 K).

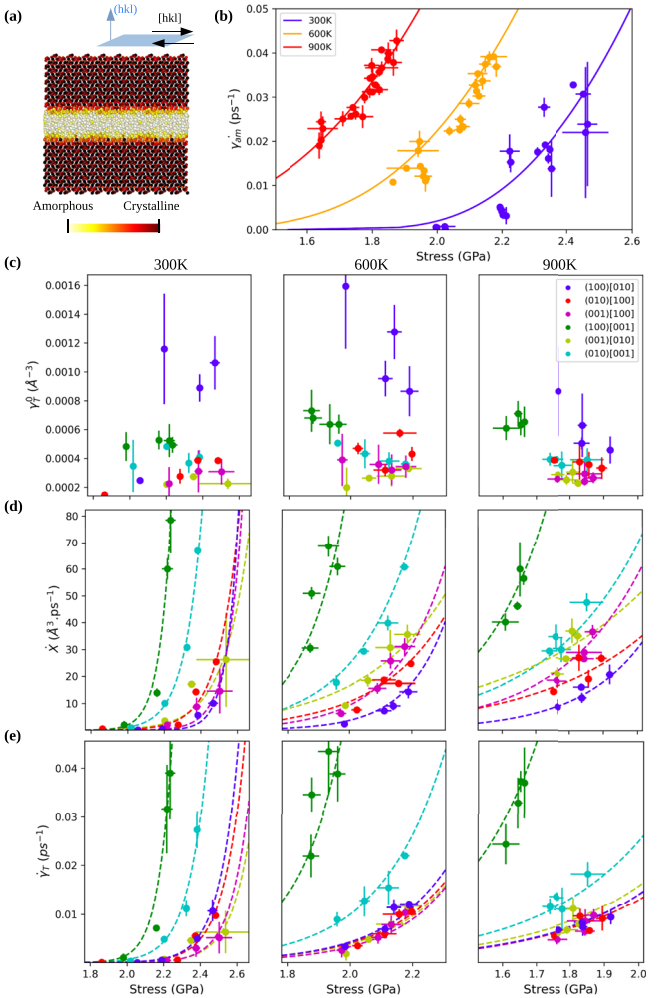

Fig. 3 | Effect of stress and temperature on a-TRIP. a Schematic of the molecular dynamics simulations constituting the data presented in this figure, the sampled (hkl) sheared planes were (100), (010) and (001) associated with [hkl] shear directions along [100], [010] and [001], for each configuration 3 different initial amorphous thickness were considered, for each system, 4 constant shear stress varying between 2 and 2.6 GPa were sampled at 300, 600 and 900 K and all systems were maintained at 0 GPa isostatic pressure during the simulation, (**b**) shear strain rate versus shear stress in the amorphous region for different temperatures, the lines represent our reparameterization of the flow law of[33], (**c**–**e**) represent respectively the reference a-TRIP shear strain (γ_T^0), the phase transformation rate ($\dot{X}$) and the a-TRIP shear strain rate ($\dot{\gamma}_T$) as a function of shear stress for different configurations and temperatures, points and error bars represent respectively the average and standard deviation over different initial amorphous thicknesses. Dotted lines in (**d**, **e**) represent the fit of the data by Eq. (3).

The calculation of the shear stress and strain rate in the amorphous region ($\dot{\gamma}_{am}$ corresponding to $\dot{\gamma}_B$ in Eq. (1)) confirms that the amorphous region follows the bulk flow law of the amorphous forsterite glass (Fig. 3b)[33]. Focusing on the amorphization process and the shear strain produced at the amorphous/crystal interface region, a convenient way to express the shear strain rate produced by the a-TRIP mechanism $\dot{\gamma}_T$(ps^{-1}) is to decompose it into a reference a-TRIP shear strain γ_T^0(Å^{-3}) and a phase transformation (i.e. amorphization) rate $\dot{X}$(Å^3.ps^{-1}) such that[17]:

$$\dot{\gamma}_T = \gamma_T^0 \dot{X} \tag{2}$$

By tracking, for all intragranular amorphous band configurations mentioned above, the evolution of strain in the amorphous/crystal interface regions as amorphization proceeds, we first find a linear relationship between this strain and the amorphous volume with a high degree of

correlation (R^2 >0.9) for the large majority (>75%) of the 270 configurations investigated; see Supplementary Fig. S.2). Considering that $\dot{\gamma}_T$ is equal to the strain rate at the amorphous/crystal interface region and time-integrating Eq. (2), the slope of the strain at amorphous/crystal interface versus amorphous volume directly gives the reference a-TRIP shear strain γ_T^0, as presented in Fig. 3c. This reference a-TRIP shear strain γ_T^0 is then found to be independent of temperature, shear stress and orientation (with an average value of 4.10^{-4} Å^{-3}) except for the (100)[010] system for which much higher values (average of 1.10^{-3} Å^{-3}) are measured, and to a lesser extend (100)[001]. To evaluate $\dot{X}$, we tracked the evolution of the amorphous volume (X) with time (t), and again observed a linear relationship between X and t (the majority of the configurations yielding to a correlation coefficient R^2 >0.9, see Supplementary Fig. S.2).

For a given crystallographic system, the amorphization rate increases with stress and temperature (see Fig. 3d) following an Arrhenius type expression:

$$\dot{X} = \dot{X}_0 e^{-\frac{Q-\tau V^\star}{RT}}, \quad (3)$$

where $\dot{X}_0$ is the reference amorphization rate, Q the activation energy, τ the shear stress, $V^\star$ the activation volume, R the gas constant and T the temperature. Fitting Eq. (3) for the different crystallographic systems yields to an average value of 74.8 ± 16.5 kJ.mol^{-1} for the activation energy and 27.5 ± 6.7 cm^3.mol^{-1} for the activation volume. This relatively low activation energy value confirms that amorphisation is essentially stress-driven. When comparing the reference a-TRIP shear strains, the (100)[010] system has the lowest amorphization rate, while the (100)[001] system has the highest amorphization rate followed by the (010)[001] system and the other systems yielding almost same values.

Since the reference a-TRIP shear strain is almost constant between systems, the behavior of a-TRIP shear strain rate $\dot{\gamma}_T$ is dominated by that of the amorphization rate and could also be described by an Arrhenius-type expression with the same mean activation energy and volume (see Fig. 3e). The systems with the highest a-TRIP shear strain rate are those with the highest amorphization rate, with significantly more shear strain released in the (100)[001] system—surpassing that of the amorphous region—followed by the (010)[001] and other systems that accommodated less plastic strain.

This small-scale investigation of stress-induced amorphization highlights a key features of the a-TRIP effect in forsterite that is the pronounced orientation effect in plastic flow, which depends on the sheared plane and direction.

Amorphization of GB in Mg_2SiO_4 polycrystals

To assess the relevance of the a-TRIP features, derived from the study of intracrystalline amorphous shear bands, to general GBs found in polycrystals, we further examined several amorphizing GBs within the polycrystalline shear deformation simulation shown in Fig. 1b, c. By focusing on GBs undergoing amorphization, we track the evolution of the crystallographic orientation of the GB planes as deformation occurs, as shown in Fig. 4 for two of these GBs (other analyzed GBs could be found in Supplementary Fig. S.3). Since amorphization occurring in the (100) and (010) planes along the [001] direction gives the highest plastic shear strain, we defined three crystallographic parameters: two representing the proximity of the GB planes to the (100) and (010) planes (shown in red and blue in Fig. 4, respectively), and one reflecting the alignment of the [001] direction with the shear direction (shown in green in Fig. 4). It is important to note that these three parameters are different in the two grains that make up the amorphized GB (solid and dotted lines in Fig. 4). Details of the methodology used to extract and track these GBs from MD simulation during shear deformation can be found in the Methods section 2.1.

This analysis firstly shows that GB amorphization in polycrystalline context is accompanied by significant rotation of the boundaries during deformation. In particular, some of these rotations do not align the GB plane with the macroscopic shear plane such as for the GB misoriented of 15.1° about [17 29 15] axis presented in Fig. 4a. This GB, which has initial crystallographic orientation very close to the (100)[001] system, is undergoing early amorphization. In fact, this orientation facilitates the generation of significant plastic strain through the a-TRIP, which explains its earlier amorphization. However, as this GB rotates during the amorphization process, its orientation deviates from the (100)[001] configuration, resulting in no further amorphization once it has rotated (i.e., the amorphous thickness remains nearly constant after the rotation).

Second, and perhaps more notably, other GBs initially oriented away from the optimal orientations (i.e., (100)[001] or (010)[001]) undergo later amorphization such as the GB misoriented of 169.9° about [40 5 $\bar{4}\bar{4}$] axis,

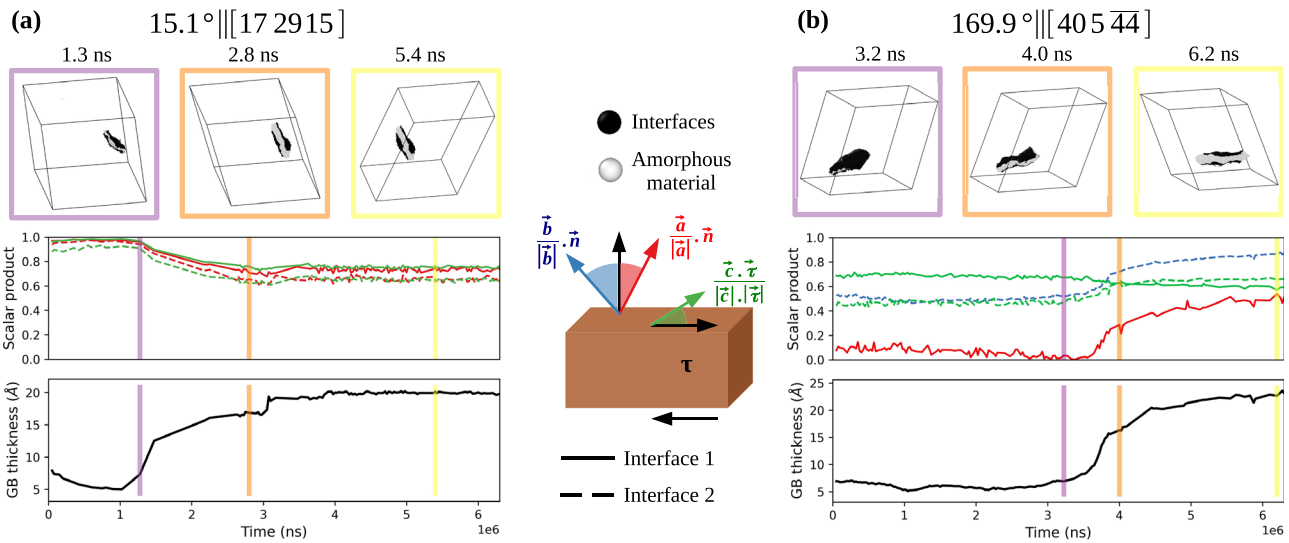

Fig. 4 | Impact of a-TRIP in polycrystals. Time evolution of two individual GB during the MD simulation of polycrystal shear deformation presented in Fig. 1b and c, (**a**) case of a GB misoriented of 15.1° about [17 29 15] axis, (**b**) case of a GB misoriented of 169.9° about [40 5 $\bar{4}\bar{4}$] axis. The upper figures represent the state of the GB at different times, with ions belonging to amorphous crystal interface and amorphous local atomic environments highlighted in black and white, respectively. The central figures represent the time evolution of the crystallographic orientation of the GB planes, where blue and red curves correspond respectively to the normalized scalar product of (010), (100) normals with the GB normal, the green curves represent the normalized scalar product of the [001] direction with the shear direction, the full and dashed lines represent the first and second GB plane, respectively. The bottom figures represent the time evolution of the amorphous thickness.

shown in Fig. 4b. Moreover, the rotations accompanying the amorphization tend to increase the proximity of the GB planes with optimal orientations for a-TRIP. This observation suggests that GB rotation during amorphization is attracted toward the optimal orientations that maximize plastic strain generation via the a-TRIP mechanism. Other examples of these two mechanisms (i.e., earlier amorphization of optimally-oriented GB, and later amorphization of away-oriented GB followed by rotation through optimal orientation) are presented in Supplementary Fig. S.3.

These results provide new insights into the features observed in HRTEM images of the amorphized olivine GBs, as shown in Fig. 1a. In fact, our results suggest that the GB plane, initially aligned with the (120) orientation, develops (010) and (100) facets during amorphization, as these orientations permit a-TRIP to generate maximum plastic strain. This mechanically driven reshaping of the GB is unexpected and can be understood in the context of the orientation effect associated with stress-induced amorphization in Mg_2SiO_4.

We expect these conclusions to extend to other materials undergoing stress-induced amorphization, where amorphous shear bands often form along orientations that deviate from the maximum shear plane. For example, in laser-shocked boron carbide, amorphous bands have been reported on planes slightly offset from the maximum shear plane, specifically the (215) and $(2\bar{2}1)$ planes[34]. In the light of the a-TRIP mechanism, amorphization along such planes may accommodate substantially more plastic strain, making them more favorable to amorphize despite not coinciding with the maximum shear plane. Similar behavior has been observed in other cases of stress-induced amorphization—for instance, in silicon, where the (112), (110), and (111) planes may maximize a-TRIP activity[35]—and, more broadly, in covalently bonded crystals[36].

Conclusion

Through combined HRTEM observations, MD, and FE simulations, we have demonstrated that stress-induced amorphization exhibits the defining features of the TRIP effect. This includes, first, substantial plastic flow originating from the crystal-to-amorphous phase transformation, localized at the transformation front. Second, a weakening of the mechanical properties of the material during the phase transformation. We further showed that a-TRIP in Mg_2SiO_4 is associated with a strong orientation effect, which leads either to reshaping of the amorphous GBs (e.g., faceting of the amorphous shear band) or to the rotation of GBs toward configurations where the (100) or (010) planes align with the [001] shear direction. This GB realignment allows the system to maximize plastic strain through stress-induced amorphization. Based on the morphology of amorphous shear bands in other materials[34,35], we believe that the conclusions we draw from our results in forsterite apply to other materials subjected to stress-induced amorphization.

Thus, our findings support the adoption of the TRIP conceptual framework to study and exploit stress-induced amorphization in materials engineering. Specifically, our results indicate that certain crystallographic planes and directions produce greater plastic strain through stress-induced amorphization. By increasing the density and optimizing the spatial distribution of these orientations during material processing, mechanical properties can be improved by exploiting stress-induced amorphization. This mechanically driven GB engineering is particularly promising for improving the toughness of materials that are typically characterized by brittle behavior.

Methods

Transmission electron microscopy

HRTEM micrographs were acquired using an aberration-corrected cubed FEI-Titan electron microscope at an operating voltage of 300 kV. Specimens are described in refs. 37, [1].

Simulation methods

Molecular dynamics. MD simulations are performed with the LAMMPS software[38]. Calculations are carried out using the rigid-ion potential developed by Pedone and co-workers[39], which includes long-range Coulomb interactions, and where a Morse function mimics short-range interactions. This interatomic potential accurately reproduces the physical properties of forsterite crystal[40], and was used recently to model tilt[41] and twist GB[42] in forsterite. In all simulations, 3D periodic boundary conditions are applied. Coulomb interactions are computed using the particle-particle/particle-mesh (pppm) method[43], and we used an integration timestep of 2 fs.

Polycrystalline MD simulation. The Mg_2SiO_4 polycrystalline sample studied here corresponds to 8 grains of random orientations for a total number of 1,477,700 ions. The initial configuration, constructed using the atomsk software[44] is first relaxed using molecular statics before being submitted to a thermalization at 300 K in the NPT ensemble during 25 ps. The as-thermalized system is finally sheared along one direction at a constant shear rate of 10^8 s^{-1} during 6.3 ns in the NVT ensemble.

Intragranular amorphous band growth simulations. The MD simulations presented in section 2 result from the systematic investigation of the mechanical behavior of an intragranular amorphous layer as a function of shear stress and temperature. Three different intragranular configurations have been modeled, corresponding to the intragranular amorphous layers lying either with the (100), (010) or (001) planes. The initial configurations of these systems are constructed by inserting a relaxed amorphous layer between two oriented crystals (amorphous thicknesses between 5 and 30 Å have been investigated). For each as-build system (containing approximately 7500 ions), we sampled two shear directions corresponding to the in-plane crystallographic directions (e.g., [010] and [001] directions for (100) plane). The shear is applied by imposing constant shear stresses of 2, 2.2, 2.4 and 2.6 GPa using the NPT ensemble (T = 300, 600 and 900 K) as implemented in LAMMPS. A total of 270 MD simulations have therefore been performed.

The atomic configuration of the MD simulation presented in section 1, consisting in a (100)-oriented amorphous layer sheared in the [001] one direction, is similar to the intragranular amorphous band system described above. However, in order to reduce temperature or stress fluctuation, it corresponds to a larger system size with approximately 150,000 ions. Indeed, such large system have been considered for direct comparison with finite element (FE) modeling. Comparison between MD and FE models further involves constant shear strain rate calculations (10^{10} s^{-1}) perfomed at 300 K.

Finite elements method. Finite element (FE) simulations are carried out using a P1+/P1 mixed velocity-pressure formulation capable to account for elastic anisotropy[45]. This framework is coupled to a crystal plasticity implementation providing the material behavior to the FE resolution, i.e., here the elastic behavior of forsterite crystal and the viscoelastic behavior of amorphous forsterite. The first is done through the crystal plasticity formalism by affecting to the crystal points very high critical resolved shear stresses for all slip systems, effectively preventing plasticity and leading to a purely elastic material. The elastic constants used are directly computed from MD simulations using the same interatomic potential. The description of the mechanical behavior of the amorphous material is implemented in the same crystal plasticity framework which allows to consider an additional relaxation mechanism covering the deformation space which cannot be accommodated by dislocation glide (i.e., reduced crystal plasticity framework[46,47]). The amorphous material is thus considered in this framework as a crystal without any slip systems, only deforming plastically through the relaxation mechanism which is expressed by a Von-Mises type equation:

$$\varepsilon^{irel} = L_{eq}^{sym}\left(\frac{S_{eq}}{\sigma_c}\right)^n, \tag{4}$$

where $L_{eq}^{sym} = \sqrt{\frac{2}{3}L^{sym} : L^{sym}}$ (: represents the double dot product) where L^{sym} is the symmetric part of the velocity gradient tensor, $S^{eq} = \sqrt{\frac{3}{2}S : S}$

where S is the deviatoric stress tensor, n is an exponent taken equal to 10 ensuring a smooth transition between elastic and plastic regime. σ_c could be seen as the strength of the relaxation mechanism and is directly computed from an Herschel-Bulkley model[48] calibrated using MD simulation of amorphous forsterite with the same interatomic potential[33]:

$$\sigma_c = a_0 + a_1(L_{eq}^{sym})^m - a_2 T\left(ln\left(\frac{a_3 T^{\frac{5}{6}}}{L_{eq}^{sym}}\right)\right)^{\frac{2}{3}} \quad (5)$$

where, a_0 = 2.5 GPa, a_1 = 2.6 GPa.ps^{-m}, m = 0.54, a_2 = 0.0038 GPa.K$^{3/2}$ and a_3 = 0.053 ps.K$^{6/5}$ are the parameters of the Herschel-Bulkley model and T is the temperature in K. The elastic constants used to describe the elastic behavior of amorphous forsterite are also extracted from MD simulation.

It is worth noticing that amorphization process is not explicity modeled within our FE framework. Instead, the evolution of amorphous thickness region in FE simulations are updated from the tabulation of the positions of the different regions (i.e. crystal, interface crystal/amorph and amorphous band) accordingly to the MD simulations. Thus, the crystal and amorphous regions needed to infer the material properties, as well as the regions in which average strain and stress are computed, are directly extracted from the tables and updated at each timestep of the FE simulation. Our FE framework does not rely on periodic boundary conditions, instead, we rely on a large FE simulation domain from which only the central part is extracted. The deformation is applied by imposing a constant velocity to the upper part of the simulation cell and by fixing the lower part. The initial FE mesh for all simulations are therefore composed of approximately 200,000 tetragonal elements with a typical element size of 2 Å. After every 1% of macroscopic shear strain, adaptative remeshing is performed in order to conserve high quality elements.

Simulation analysis

In all MD simulations presented here, the local shear stresses and strains are computed following the same methodology. Moreover, the different parts of the analysis have been performed using the AtomHIC home-made code (https://github.com/JeanFurstoss/AtomHIC/releases).

The shear stress τ^α in a given region α is computed such that:

$$\tau^\alpha = \frac{\sum^{i\in\Omega^\alpha}\sigma^i_{ab}}{\sum^{i\in\Omega^\alpha}V^i}, \quad (6)$$

where Ω^α represents the set of ions belonging to region α, σ^i_{ab} represents the ab component of the atomic stress tensor of ion i, where a represents the direction normal to the amorphous plane and b the shear direction. V^i represents the atomic volume considered as the volume of the Voronoi cell around the ion.

The shear strain γ^α in a given region α is computed as:

$$\gamma^\alpha = \sum^{i\in\Omega^\alpha}\varepsilon^i_{ab}/N^\alpha, \quad (7)$$

where N^α is the number of ions in region α and ε^i_{ab} is the ab component of the atomic strain, which is computed following the methodology of Shimizu[49] as implemented in the OVITO software[50]. The reference atomic configuration needed for the calculation of the atomic strain tensor is taken as the atomic configuration 4 ps before the analyzed configuration, meaning that the shear strain rate could be expressed as $\gamma^\alpha/4$ (in ps^{-1}). The cutoff radius for the calculation of the atomic strain is taken equal to 5 Å, which allows from Eq. (7) applied to the whole system to retrieve the macroscopic shear strain (i.e., the one of the simulation cell).

Polycrystal MD simulation analysis. The structural analysis of the polycrystal is performed using the Steinhardt Gaussian Mixture Analysis (SGMA)[32] recently developed and applied to the identification of dislocations and GB in forsterite. The SGMA used here has been trained on a dataset containing strained forsterite perfect crystals, [100] and [001] screw dislocations, Mg_2SiO_4 amorphous bulk state and amorphous/crystal interface, which allows in the polycrystalline system to distinguish these different local atomic environments.

Once the structural analysis is performed, individual GB composed by the amorphous/crystal interface regions and amorphous band are tracked over time. The GBs with less than 500 ions are discarded from the analysis. For each GB, the eigenvector with the smallest eigenvalue of the best-fitting 3D Gaussian distribution gives the GB plane-normal direction. The crystal orientations are tracked over time using tagged ions in each grains, which allows to get the crystallographic plane normal of each amorphous/crystal interface.

Analysis of small and large-scale MD simulations. The intragranular amorphous band MD simulations, either performed at constant strain rate or at constant applied shear stress, have been analyzed using the same methodology. The main goals of this analysis is to extract the amorphous thickness as well as the shear strain and stress in the different part of the system, namely the crystal, the amorphous band and the amorphous/crystal interface.

This is done by first computing a recently developed order parameter[42] allowing to discriminate perfect crystal from disordered local atomic environment in forsterite (see Fig. 5a). The one dimensional density of this order parameter is then computed in the direction normal to the amorphous

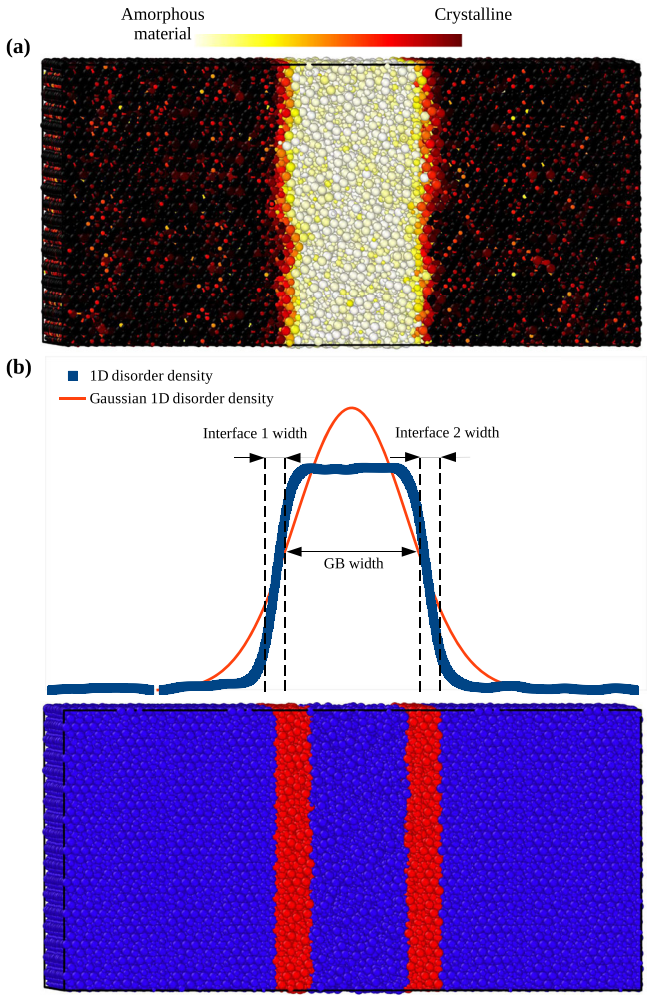

Fig. 5 | Extraction of amorphous/crystal interface. a Example of an intragranular amorphous band. Ions are displayed with a color coding reflecting the local atomic disorder environment (**b**) 1d order parameter density from MD simulation (blue curve) and fitted by Gaussian distribution (orange), the amorphous thickness is inferred from the full width at half maximum and the ions belonging to the amorphous/crystal interfaces (red ions in the bottom figure) are identified using the 1D density profile (see text).

plane and fitted by a Gaussian distribution (see Fig. 5b). The amorphous thickness is then computed as the full width at half maximum of the Gaussian distribution.

The first step needed for the calculation of stress and strain in the different part of the system is to identify which ions belong to the different zones. To do so, we search for positions corresponding to an increase/decrease of 20% from the minimum/maximum of density of the order parameter and affect ions between these positions to the zone corresponding to the crystal/amorph interface such as shown in Fig. 5b. The identification of ions in the other parts of the system (crystals and amorph regions) is then straightforward.

In order to plot the data in the $(\tau, \dot{\gamma})$ space, we need to average the shear stress and strain over time for each simulation. This averaging is performed after the system reach 20% of shear strain, preventing bias from elastic regime and hardening/softening effect at the beginning of mechanical load and effectively capturing quasi-steady state regime.

Data availability

All the data used for plotting the different figures presented in this work, as well as the LAMMPS scripts used for the different computations and the associated dump files, are available from the authors upon request.

Code availability

All the numerical analysis presented in this work have been performed using the AtomHIC code which is freely available at https://github.com/JeanFurstoss/AtomHIC/releases.

Received: 3 October 2025; Accepted: 5 December 2025;
Published online: 22 January 2026

References

1. Samae, V. et al. Stress-induced amorphization triggers deformation in the lithospheric mantle. *Nature* **591**, 82–86 (2021).
2. Idrissi, H., Carrez, P. & Cordier, P. On amorphization as a deformation mechanism under high stresses. *Curr. Opin. Solid State Mater. Sci.* **26**, 100976 (2022).
3. Hu, X. et al. Amorphous shear bands in crystalline materials as drivers of plasticity. *Nat. Mater.* **22**, 1071–1077 (2023).
4. Tan, J. et al. Deformable monoclinic gallium telluride with high in-plane structural anisotropy. *Mater. Today* **80**, 250–261 (2024).
5. Reddy, K. M., Liu, P., Hirata, A., Fujita, T. & Chen, M. Atomic structure of amorphous shear bands in boron carbide. *Nat. Commun.* **4**, 2483 (2013).
6. Zhao, S. et al. Shock-induced amorphization in silicon carbide. *Acta Materialia* **158**, 206–213 (2018).
7. Luo, H. et al. Plasticity without dislocations in a polycrystalline intermetallic. *Nat. Commun.* **10**, 3587 (2019).
8. Wang, H. et al. Deformation-induced crystalline-to-amorphous phase transformation in a crmnfeconi high-entropy alloy. *Sci. Adv.* **7**, eabe3105 (2021).
9. Gratz, A. et al. Shock metamorphism of quartz with initial temperatures- 170 to+ 1000°C. *Phys. Chem. Miner.* **19**, 267–288 (1992).
10. Idrissi, H. et al. On the formation mechanisms of intragranular shear bands in olivine by stress-induced amorphization. *Acta Materialia* **239**, 118247 (2022).
11. Xu, Y. et al. Shear localization and recrystallization in dynamic deformation of 8090 Al–Li alloy. *Mater. Sci. Eng.: A* **299**, 287–295 (2001).
12. Heera, V. et al. Density and structural changes in sic after amorphization and annealing. *Appl. Phys. Lett.* **70**, 3531–3533 (1997).
13. An, Q. & Goddard III, W. A. Atomistic origin of brittle failure of boron carbide from large-scale reactive dynamics simulations: Suggestions toward improved ductility. *Phys. Rev. Lett.* **115**, 105501 (2015).
14. Luo, H., Zhang, H., Sheng, H., Liu, J. P. & Szlufarska, I. Amorphous shear bands in smco5. *Mater. Sci. Eng.: A* **785**, 139340 (2020).
15. Greenwood, G. W. & Johnson, R. The deformation of metals under small stresses during phase transformations. *Proc. R. Soc. Lond. Ser. A. Math. Phys. Sci.* **283**, 403–422 (1965).
16. Magee, C. L. Transformation kinetics, microplasticity and aging of martensite in Fe-31 Ni, Ph. D. Thesis, Carnegie Institute of Technology, Pittsburgh (1966).
17. Poirier, J. On transformation plasticity. *J. Geophys. Res.: Solid Earth* **87**, 6791–6797 (1982).
18. Taleb, L., Cavallo, N. & Waeckel, F. Experimental analysis of transformation plasticity. *Int. J. Plasticity* **17**, 1–20 (2001).
19. Schmidt, C., Bruhn, D. & Wirth, R. Experimental evidence of transformation plasticity in silicates: minimum of creep strength in quartz. *Earth Planet. Sci. Lett.* **205**, 273–280 (2003).
20. Dunand, D. C., Schuh, C. & Goldsby, D. L. Pressure-induced transformation plasticity of H_2O ice. *Phys. Rev. Lett.* **86**, 668 (2001).
21. Soleimani, M., Kalhor, A. & Mirzadeh, H. Transformation-induced plasticity (trip) in advanced steels: a review. *Mater. Sci. Eng.: A* **795**, 140023 (2020).
22. Eggeler, G., Hornbogen, E., Yawny, A., Heckmann, A. & Wagner, M. Structural and functional fatigue of NiTi shape memory alloys. *Mater. Sci. Eng.: A* **378**, 24–33 (2004).
23. Leblond, J.-B., Devaux, J. & Devaux, J. Mathematical modelling of transformation plasticity in steels I: Case of ideal-plastic phases. *Int. J. Plasticity* **5**, 551–572 (1989).
24. Fischer, F., Sun, Q.-P., Tanaka, K. Transformation-induced plasticity (trip) (1996).
25. Kranjc, K. et al. Amorphization and plasticity of olivine during low-temperature micropillar deformation experiments. *J. Geophys. Res.: Solid Earth* **125**, e2019JB019242 (2020).
26. Carter, N. L. & Ave'Lallemant, H. G. High temperature flow of dunite and peridotite. *Geol. Soc. Am. Bull.* **81**, 2181–2202 (1970).
27. Mussi, A., Cordier, P., Demouchy, S. & Vanmansart, C. Characterization of the glide planes of the [001] screw dislocations in olivine using electron tomography. *Phys. Chem. Miner.* **41**, 537–545 (2014).
28. Mussi, A., Nafi, M., Demouchy, S. & Cordier, P. On the deformation mechanism of olivine single crystals at lithospheric temperatures: an electron tomography study. *Eur. J. Mineral.* **27**, 707–715 (2015).
29. Durinck, J., Devincre, B., Kubin, L. & Cordier, P. Modeling the plastic deformation of olivine by dislocation dynamics simulations. *Am. Mineralogist* **92**, 1346–1357 (2007).
30. Hirth, G. & Kohlstedt, D. L. Experimental constraints on the dynamics of the partially molten upper mantle: 2. deformation in the dislocation creep regime. *J. Geophys. Res.: Solid Earth* **100**, 15441–15449 (1995).
31. Cordier, P. et al. Disclinations provide the missing mechanism for deforming olivine-rich rocks in the mantle. *Nature* **507**, 51–56 (2014).
32. Furstoss, J., Salazar, C. R., Carrez, P., Hirel, P. & Lam, J. All-around local structure classification with supervised learning: The example of crystal phases and dislocations in complex oxides. *Computer Phys. Commun.* **309**, 109480 (2025).
33. Delbecq, V., Carrez, P. & Cordier, P. Rheological properties of Mg_2SiO_4 glass: A molecular dynamics study. *J. Non-Crystalline Solids* **619**, 122572 (2023).
34. Zhao, S. et al. Directional amorphization of boron carbide subjected to laser shock compression. *Proc. Natl. Acad. Sci.* **113**, 12088–12093 (2016).
35. Chen, H., Levitas, V. I. & Xiong, L. Amorphization induced by 60 shuffle dislocation pileup against different grain boundaries in silicon bicrystal under shear. *Acta Materialia* **179**, 287–295 (2019).
36. Zhao, S. et al. Directional amorphization of covalently-bonded solids: A generalized deformation mechanism in extreme loading. *Mater. Today* **49**, 59–67 (2021).
37. Gasc, J., Demouchy, S., Barou, F., Koizumi, S. & Cordier, P. Creep mechanisms in the lithospheric mantle inferred from deformation of

iron-free forsterite aggregates at 900–1200°C. *Tectonophysics* **761**, 16–30 (2019).
38. Plimpton, S. Fast parallel algorithms for short-range molecular dynamics. *J. Computational Phys.* **117**, 1–19 (1995).
39. Pedone, A., Malavasi, G., Menziani, M. C., Cormack, A. N. & Segre, U. A new self-consistent empirical interatomic potential model for oxides, silicates, and silica-based glasses. *J. Phys. Chem. B* **110**, 11780–11795 (2006).
40. Hirel, P., Furstoss, J. & Carrez, P. A critical assessment of interatomic potentials for modelling lattice defects in forsterite Mg_2SiO_4 from 0 to 12 GPa. *Phys. Chem. Miner.* **48**, 46 (2021).
41. Furstoss, J., Hirel, P., Carrez, P. & Cordier, P. Complexions and stoichiometry of the 60.8°//[100](011) symmetrical tilt grain boundary in Mg_2SiO_4 forsterite: A combined empirical potential and first-principles study. *Am. Mineralogist* **107**, 2034–2043 (2022).
42. Furstoss, J. et al. Structures and energies of twist grain boundaries in Mg_2SiO_4 forsterite. *Computational Mater. Sci.* **233**, 112768 (2024).
43. Eastwood, J. W., Hockney, R. W. & Lawrence, D. P3m3dp—the three-dimensional periodic particle-particle/particle-mesh program. *Computer Phys. Commun.* **19**, 215–261 (1980).
44. Hirel, P. Atomsk: A tool for manipulating and converting atomic data files. *Computer Phys. Commun.* **197**, 212–219 (2015).
45. Furstoss, J., Ruiz Sarrazola, D. A., Bernacki, M. & Pino Muñoz, D. Handling tensors using tensorial kelvin bases: application to olivine polycrystal deformation modeling using elastically anistropic cpfem. *Computational Mech.* **67**, 955–967 (2021).
46. Maresca, F., Kouznetsova, V. & Geers, M. Reduced crystal plasticity for materials with constrained slip activity. *Mech. Mater.* **92**, 198–210 (2016).
47. Furstoss, J., Petit, C., Ganino, C., Bernacki, M. & Pino-Muñoz, D. A new finite element approach to model microscale strain localization within olivine aggregates. *Solid Earth Discuss.* **2021**, 1–29 (2021).
48. Chattoraj, J., Caroli, C. & Lemai^tre, A. Universal additive effect of temperature on the rheology of amorphous solids. *Phys. Rev. Lett.* **105**, 266001 (2010).
49. Shimizu, F., Ogata, S. & Li, J. Theory of shear banding in metallic glasses and molecular dynamics calculations. *Mater. Trans.* **48**, 2923–2927 (2007).
50. Stukowski, A. Visualization and analysis of atomistic simulation data with ovito–the open visualization tool. *Model. Simul. Mater. Sci. Eng.* **18**, 015012 (2009).

Acknowledgements

This project has received funding from the European Research Council (ERC) under the European Union's Horizon 2020 research and innovation program under grant agreement No. 787198 - TimeMan. This project has received funding from the French government through the Programme Investissement d'Avenir (I-SITE ULNE / ANR-16-IDEX-0004 ULNE) managed by the Agence Nationale de la Recherche, under the project name NuMoGO. Computational resources have been provided by the DSI at Université de Lille. H. Idrissi is mandated by the Belgian National Fund for Scientific Research (FSR- FNRS).

Author contributions

The HRTEM was performed by H.I. and V.S. The MD simulations were performed by V.D. and J.F. The FE simulations were performed by D.P.M. and J.F. The analysis of the different simulations was performed by J.F. The project was supervised by P.Cor. The manuscript was written by J.F., D.P.M., P.Car., P.H., and P.Cor. with input from all authors.

Competing interests

The authors declare no competing interests.

Additional information

Supplementary information The online version contains supplementary material available at https://doi.org/10.1038/s43246-025-01038-0.

Correspondence and requests for materials should be addressed to Jean Furstoss.

Peer review information *Communications Materials* thanks the anonymous reviewers for their contribution to the peer review of this work. A peer review file is available.